Ocean Dynamics (2013) 63:577–587
DOI 10.1007/s10236-013-0610-8

Contrasting the evolution between two types of El Niño in a data assimilation model

Chau-Ron Wu · Li-Chiao Wang

Received: 28 August 2012 / Accepted: 26 March 2013 / Published online: 13 April 2013

Abstract Simulation outputs were used to contrast the distinct evolution patterns between two types of El Niño. The modeled isotherm depth anomalies closely matched satellite sea surface height anomalies. Results for the El Niño Modoki (central Pacific El Niño) corresponded well with previous studies which suggested that thermocline variations in the equatorial Pacific contain an east–west oscillation. The eastern Pacific El Niño experienced an additional north–south seesaw oscillation between approximately 15° N and 15° S. The wind stress curl pattern over the west-central Pacific was responsible for the unusual manifestation of the eastern Pacific El Niño. The reason why the 1982/1983 El Niño was followed by a normal state whereas a La Niña phase developed from the 1997/1998 El Niño is also discussed. In 1997/1998, the Intertropical Convergence Zone (ITCZ) retreated faster and easterly trade winds appeared immediately after the mature El Niño, cooling the sea surface temperature in the equatorial Pacific and generating the La Niña event. The slow retreat of the ITCZ in 1982/1983 terminated the warm event at a much slower rate and ultimately resulted in a normal phase.

Keywords Eastern Pacific El Niño · Central Pacific El Niño (El Niño Modoki) · Wind stress curl pattern

Responsible Editor: Yukio Masumoto

This article is part of the Topical Collection on the *4th International Workshop on Modelling the Ocean in Yokohama, Japan 21–24 May 2012*

C.-R. Wu (✉) · L.-C. Wang
Department of Earth Sciences, National Taiwan Normal University, No. 88, Section 4 Ting-Chou Road, Taipei 11677, Taiwan
e-mail: cwu@ntnu.edu.tw

1 Introduction

The recharge–discharge oscillator theory (e.g., Jin 1997a, b; Meinen and McPhaden 2000) describes the El Niño–Southern Oscillation (ENSO) phenomenon as the zonal transport of warm water along the equator associated with El Niño and La Niña. The recharge and discharge can be estimated by variations in the volume of water warmer than 20 °C, also known as the warm water volume (WWV). The WWV builds up at the equator prior to El Niño and is transported to off-equatorial Pacific locations during the mature warm phase. The recharge of the WWV in the equatorial Pacific is a necessary condition for the development of El Niño (e.g., Cane et al. 1986).

Recent studies have shown that there are two types of El Niño (e.g., Ashok et al. 2007; Yu and Kao 2007; Kug et al. 2009). The 1982/1983 and 1997/1998 events were representative of the canonical eastern Pacific El Niño (EP-El Niño, Kao and Yu 2009), which is also referred to as a cold tongue El Niño (Kug et al. 2009). The more recently identified El Niño type has a distinct difference in the location of maximum sea surface temperature (SST) anomalies from the canonical El Niño. This type has been termed the El Niño Modoki (Ashok et al. 2007), as well as a central Pacific El Niño (CP-El Niño, Kao and Yu 2009), Date Line El Niño (Larkin and Harrison 2005), or Warm Pool El Niño (Kug et al. 2009). The recharge–discharge oscillator theory has been applied to these two different types of El Niño. It has been suggested that the EP-El Niño is produced by basin-wide thermocline variations, whereas the CP-El Niño involves only local air–sea interactions (e.g., Kao and Yu 2009; Kug et al. 2009; Yu and Kim 2010). These studies concluded that the EP-El Niño acts as a mechanism to remove excess heat content to off-equatorial Pacific locations and operates as proposed by the recharge–discharge theory.

The canonical ENSO recharge–discharge theory does not emphasize the important role of the wind stress curl on the recharge–discharge process (e.g., Jin 1997a, b). According to Jin's parameters (Jin 1997b), the zonal wind stress has a meridional scale that is so large that the stress remains almost constant near the equator and its curl is negligible. However, thermocline depth variations are highly related to surface wind variations, and the essential role of wind stress curl in controlling the thermocline displacement cannot be ignored. Clarke et al. (2007) also emphasized that the wind stress curl over the west-central Pacific is closely linked to equatorial thermocline variations. The wind stress curl variation and its intensity near the equatorial region trigger both zonal and meridional transports, which can explain the recharge and discharge of the WWV.

The present report is structured as follows. Section 2 describes the datasets used in this study. In Section 3 we reveal two distinct patterns of El Niño evolution and their forcing mechanisms, and explore why two different decay patterns exist for the EP-El Niño. Section 4 presents our conclusions.

2 Data

The 20 °C isotherm depth anomaly and current velocity data used in this study were based on the National Centers for Environmental Prediction (NCEP) Global Ocean Data Assimilation System (GODAS) product (Behringer and Xue 2004). The GODAS domain covers 65° N to 75° S with a resolution of 1/3°×1/3°. The temporal range extends from January 1980 to September 2010. The model has 40 levels with 10-m resolution near the sea surface and is forced by momentum, heat, and freshwater fluxes from the NCEP-Department of Energy (NCEP-DOE) reanalysis 2 (R2) (Kanamitsu et al. 2002), which is an improved version of the NCEP reanalysis 1 (R1) model with updated parameterizations of physical processes and several errors fixed. The temperature profiles assimilated in GODAS include those from the Tropical Ocean and Global Atmosphere-Tropical Atmosphere Ocean (TOGA-TAO), Pilot Research Array in the Tropical Atlantic (PIRATA), Triangle Trans-Ocean Buoy Network (TRITON) moorings (McPhaden et al. 2001), bathythermographs (XBTs), and Argo profiling floats. In addition to the temperature, a synthetic salinity profile was computed for each temperature profile using a local temperature-salinity climatology based on the annual mean fields of temperature and salinity from the National Oceanographic Data Center (NODC) World Ocean Database (Conkright et al. 1999).

Surface wind stress data from 1948 were provided by the NCEP/National Center for Atmospheric Research reanalysis project (R1) (Kistler et al. 2001) and were also used to calculate the wind stress curl. Monthly averages on global grids (2.5°×2.5°) were available from the Climate Diagnostics Center of the National Oceanic and Atmospheric Administration's (NOAA) Earth System Research Laboratory (http://www.cdc.noaa.gov/). Sea surface height anomalies were obtained from AVISO (Archiving, Validation and Interpretation of Satellite Oceanographic data; http://www.aviso.oceanobs.com) and were merged from altimeter observations by multiple satellites, including TOPEX/Poseidon, European Remote Sensing satellites 1 and 2 (ERS-1&2), Jason-1 and 2, Envisat, and Geosat Follow On (GFO). The product was gridded on a Mercator grid of 1/3°×1/3° and a time interval of 7 days, and is available from October 1992 onward.

3 Result and discussion

3.1 Simulated flow patterns associated with the two types of El Niño

The general circulation pattern of the equatorial Pacific was quite realistic in the GODAS model. Figure 1a shows the simulated mean circulation pattern of the Pacific equatorial current based on GODAS products and is consistent with the observed mean flow pattern in the region (e.g., Lukas 2001). The equatorial zonal currents consist of a westward-flowing wide-range surface current, the South Equatorial Current (SEC), which is located between about 8° S and 3° N. Following the definition of Wyrtki (1974), the SEC is further split into a northern branch (SECn) and a southern branch (SECs) at the equator. To the north, the eastward-flowing current is the North Equatorial Counter Current (NECC, between about 5° N and 10° N). North of the NECC, there is an intense westward current, the North Equatorial Current (NEC, between about 10° N and 20° N). The NEC is the southern limb of the North Pacific subtropical gyre and the upstream of the Kuroshio. The South Equatorial Counter Current extends eastward from the western boundary region, but it only intermittently reaches the central and eastern Pacific. Wang and Wu (2012) showed that the vertical profile along the equator from GODAS is quite similar to that plotted by Lukas (2001) based on the NOAA/NCEP ocean assimilation/reanalysis product. Furthermore, the annual cycle of zonal currents on the equator from GODAS is also consistent with that based on TAO array data (Wang and Wu 2012).

In addition to the mean circulation, the GODAS model reveals distinct circulation patterns between El Niño Modoki (CP-El Niño) and EP-El Niño. Figure 1b and c show the spatial circulation patterns in the equatorial Pacific composited by the mature phases of El Niño Modoki and EP-El Niño years, respectively. El Niño Modoki years include 1991/1992, 1994/1995, 2002/2003,

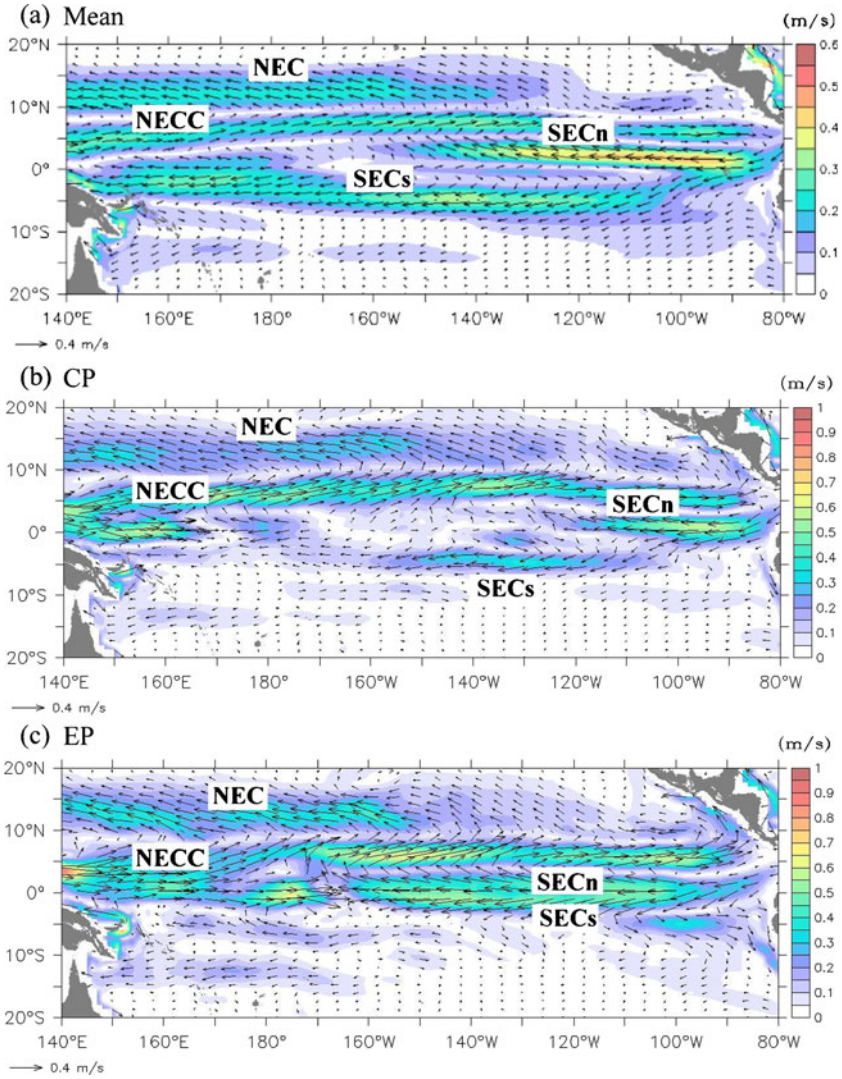

Fig. 1 **a** Mean surface circulation (averaged from 0 to 50 m) in the equatorial Pacific based on GODAS model assimilation (units: m/s). Velocity composites during the mature phase of **b** CP-El Niño events and **c** EP-El Niño events. *Shading* indicates the current intensity. Contour interval is 0.05 m/s

2004/2005, and 2006/2007. Typical EP-El Niño events occurred in 1982/1983 and 1997/1998. The phases of El Niño evolution have been defined by Kug et al. (2010). The period of the developing phase is from March to November, the mature phase is from December to February of the following year, and the decay phase is from February to October. The mean circulation in Fig. 1a shows that the SECn and SECs are clearly separated from each other. In the mature phase of El Niño Modoki, the eastward NECC strengthens while the westward SECn and SECs weaken compared with the velocity composite of normal years (Fig. 1b). The SECn becomes much weaker and is confined to the east of 125° W. The SECs is probably blocked by the shoaling Equatorial Undercurrent (EUC) and is seldom able to reach the western boundary.

The circulation during the mature phase of EP-El Niño has a distinctive pattern. The NECC and EUC merge and surge eastward (Fig. 1c). This unusual performance of the eastward currents is considered to be a great disturbance to the westward currents. The SECn and SECs also merge together and strengthen. These two merged currents moving in opposite directions match each other in strength and become deadlocked at ~165° W. This unusual pattern appears only during the EP-El Niño and is very different from the events considered in the earlier El Niño studies. Moreover, it is often observed that the NEC tends to migrate northward rather than flowing westward during an El Niño event. Figure 1c shows that the latitude of the NEC is ~16° N as it reaches the western Pacific boundary at the Philippine coast. The bifurcation point of the NEC is much farther north during an EP-El Niño than during an El Niño Modoki (CP-El Niño).

3.2 The pattern of evolution for the two types of El Niño

The pattern of evolution for the El Niño can be followed through depth changes in the equatorial Pacific thermocline. Two distinct patterns of El Niño evolution have been documented using the tropical 20 °C isotherm depth (D20) of the GODAS product. The D20 is located in the middle of the

main thermocline throughout the region (Kessler 1990; Ji and Leetmaa 1997; Braganza 2008). Figure 2 shows the typical evolution of an El Niño Modoki (CP-El Niño) in 1994/1995. CP type D20 anomalies are relatively weaker and found at depths less than 30 m. In September 1994, during the onset of a warm El Niño, a positive D20 anomaly occurred in the central and eastern Pacific (Fig. 2a). The positive anomaly expanded zonally and generated a basin-wide warming. In December 1994, when the warm event reached its mature phase, the positive D20 anomaly began to concentrate in the eastern Pacific at 5° N–5° S. A negative D20 anomaly occurred in the western Pacific, but was not as obvious (Fig. 2b). The schematic diagram in Fig. 2e demonstrates that the thermocline depth was elevated in the western Pacific but deepened in the eastern Pacific. During the decaying phase in March 1995, the positive D20 anomaly was replaced by a weak basin-wide negative D20 anomaly (Fig. 2c), tilting the thermocline toward the opposite side (Fig. 2f). When the La Niña was developing in June 1995, a negative anomaly was observed in the eastern Pacific, although it was still weak (Fig. 2d). Similar patterns of evolution have been observed in the other El Niño Modoki events (e.g., 1991/1992, 2002/2003, 2004/2005, 2006/2007, and 2009/2010).

To relate the D20 anomalies to the sea surface height pattern in the tropic Pacific Ocean, sea surface height anomalies based on AVISO satellite altimeter observations in 1994/1995 are shown in Fig. 3. The development and decay of the 1994/1995 El Niño are evident in the gridded sea surface height anomalies. A high sea surface first appeared in the east-central equatorial Pacific in September 1994 prior to the El Niño. The large and positive sea surface height anomalies extended to the eastern Pacific during the mature phase in December 1994. During the decay phase in March 1995, negative sea surface height anomalies developed in the eastern Pacific, before becoming weaker in June 1995 (Fig. 3c–d). These patterns of evolution of satellite sea surface height anomalies, which show the zonal seesaw oscillation during an El Niño Modoki, corresponded well with modeled thermocline depth variations, further validating the GODAS product.

Relatively strong thermocline depth variations were observed during the EP-El Niño event (Fig. 4). In September

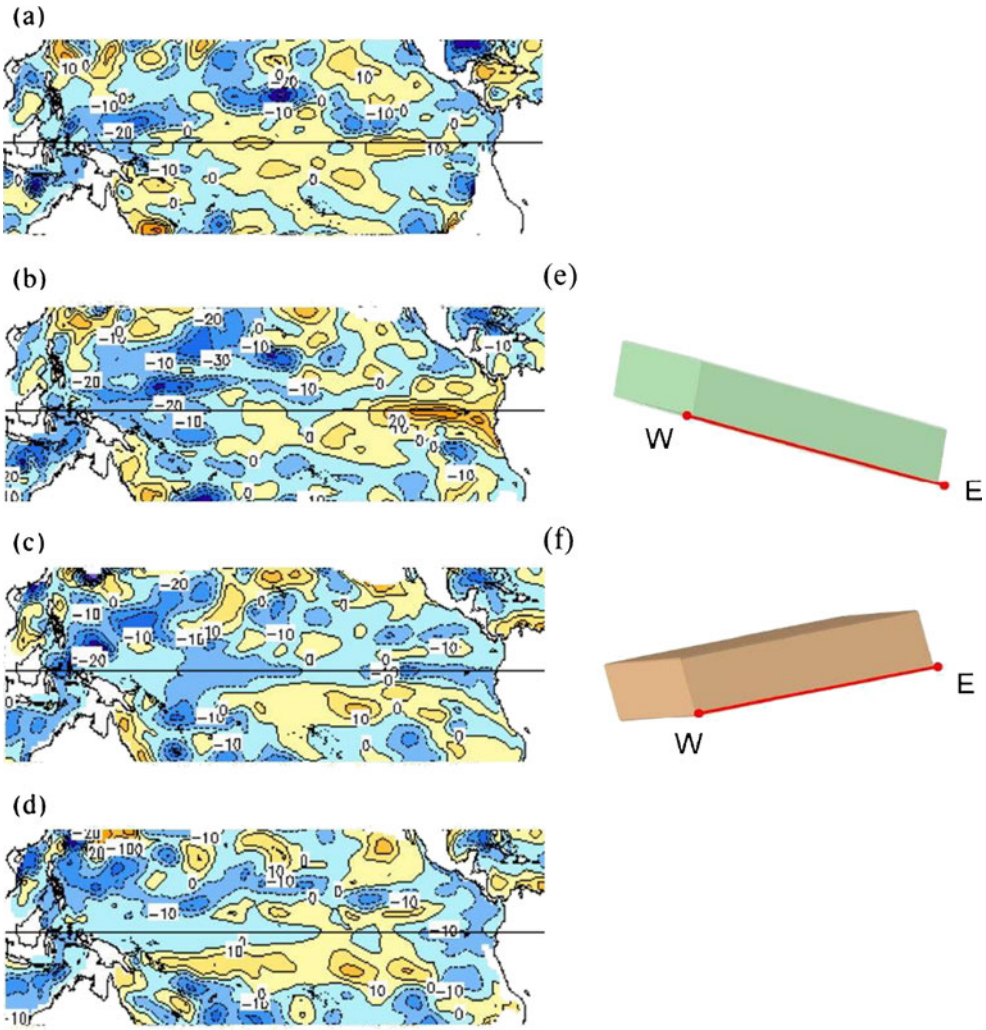

Fig. 2 The modeled 20 °C isotherm depth anomalies together with the graphs for **a** September 1994, **b** December 1994, **c** March 1995, and **d** June 1995. Contour interval for the D20 isotherm depth is 10 m. **e** Schematic diagram for (**b**) and **f** schematic diagram for (**c**)

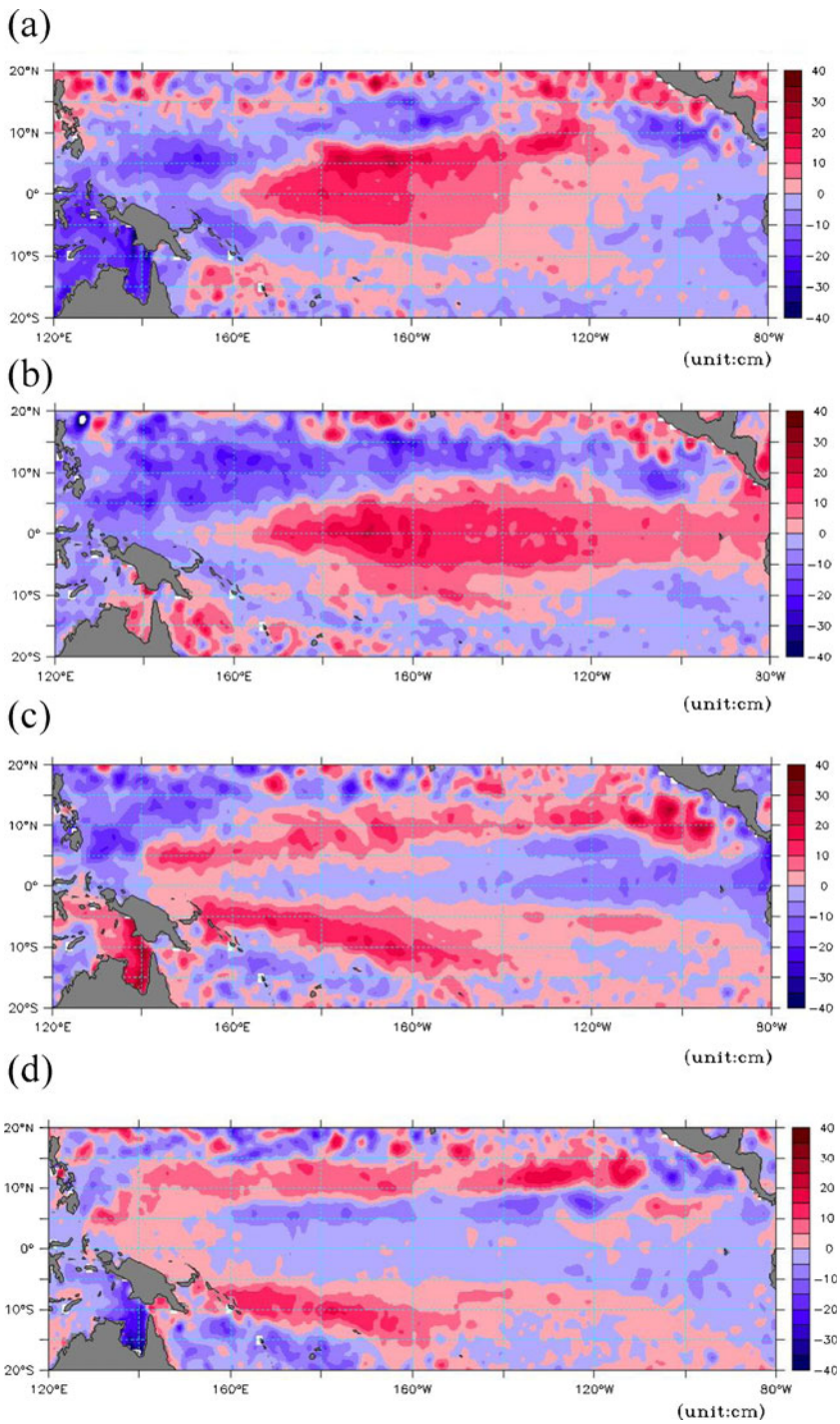

Fig. 3 Sea surface height anomalies from AVISO in **a** September 1994, **b** December 1994, **c** March 1995, and **d** June 1995. Contour interval for sea surface height anomalies is 5 cm

1997 during the onset of an EP-El Niño, a large and negative D20 anomaly (>30 m) was observed over the region 5° N–15° N, 140° E–170° E (Fig. 4a). Unlike the El Niño Modoki pattern, the D20 anomaly occurred not only around the equator, but also extended to the extratropics. This resulted in a thermocline that tended to tilt in a peculiar way. Figure 4e shows this in a schematic diagram. The thermocline in the northwestern Pacific was higher than the gradient between the eastern and western Pacific, which was observed during an El Niño Modoki. In December 1997 during the mature phase, the negative D20 anomaly had extended to the east and had become larger (>50 m; Fig. 4b). The symmetric anomaly around the equator generated a thermocline pattern similar to that in the mature phase of El Niño Modoki (Fig. 2e or Fig. 4f), except for a larger D20 anomaly gradient between the east and west Pacific. In March 1998, during the decay phase, the negative anomaly separated into two portions. One portion kept moving

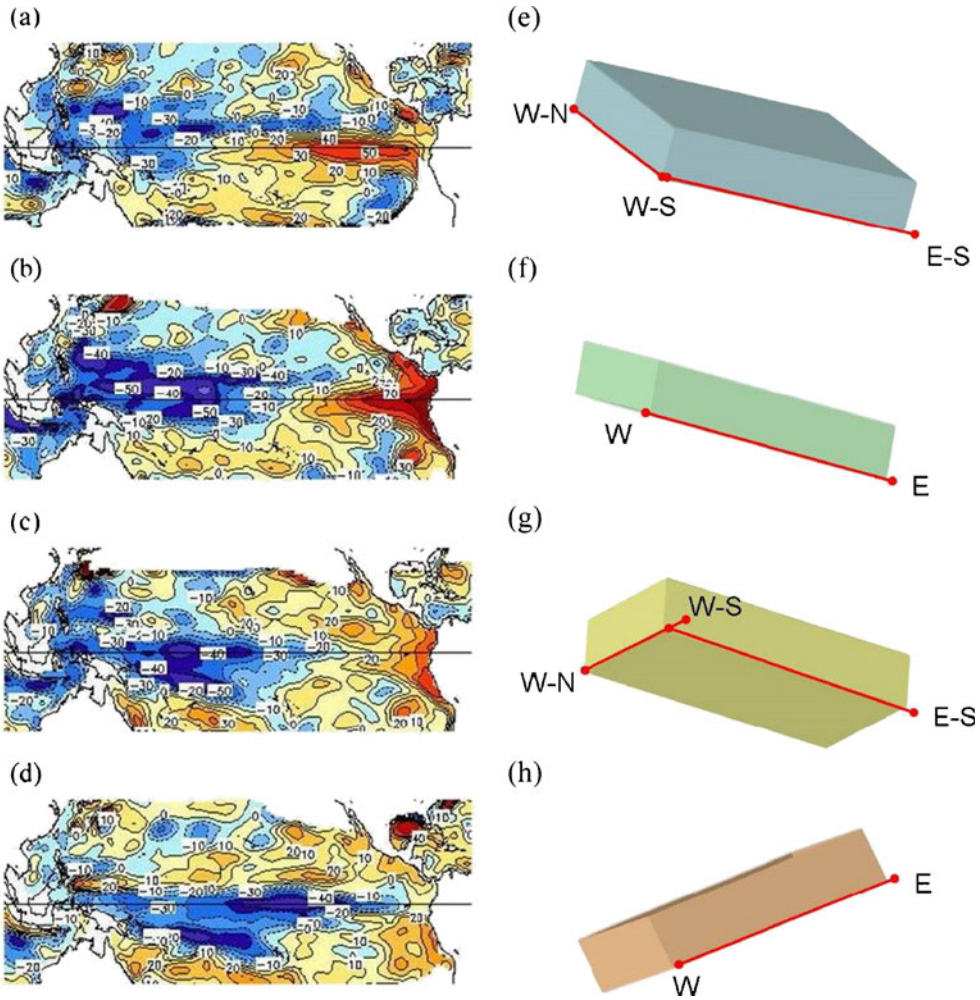

Fig. 4 Same as Fig. 2 except in **a** September 1997, **b** December 1997, **c** March 1998, and **d** June 1998, with respective schematic diagrams in **e** to **h**

southeastward and extended over the region 5° S–15° S, 160° E–150° W (Fig. 4c). Figure 4g shows that the thermocline tilted to the other side and became elevated in the southwestern Pacific (Fig. 4g). Another portion was trapped at the equator, becoming eastward-propagating Kelvin waves. The D20 fluctuations are the manifestation of Kelvin waves. The occurrence of upwelling Kelvin waves agrees with findings of previous studies (e.g., Wang et al. 1999; Luo and Yamagata 2001). In June 1998, negative D20 anomalies in the form of Kelvin waves shifted eastward to about 120° W–150° W at the equator (Fig. 4d). The negative D20 anomalies moved eastwards and raised the thermocline depth in the eastern Pacific. The thermocline depth gradient in the east–west direction was weakened or even reversed (Fig. 4h). Another recent EP type of El Niño (1982/1983) displayed a similar evolution pattern except during the decay phase. Such differences might affect SST variations and the evolution of the following La Niña, as is discussed further in Section 3.4.

The satellite-observed sea surface height anomaly patterns are also comparable to the simulated thermocline depth variations observed during the 1997/1998 EP-El Niño. Figure 5 shows a distinctly different pattern from the sea surface height anomalies observed in 1994/1995 (Fig. 3). Compared with 1994/1995, the monthly sea surface height anomaly patterns in 1997/1998 fluctuated to a larger degree. A strong and positive sea surface height developed in the central and eastern Pacific Ocean in September 1997 (Fig. 5a). It further intensified and the maximum sea surface height anomaly shifted to the eastern boundary in the mature phase of December 1997 (Fig. 5b). After the peak of the El Niño event, the positive sea surface height anomaly gradually declined (Fig. 5c–d) as previously described using satellite SST data. During its evolution, the negative sea surface height anomaly displayed a meridional oscillation in the western Pacific during EP-El Niño, similar to the development of the negative D20 anomaly. The lower sea surface height anomaly occupied the western Pacific (Fig. 5a), bifurcating into the two components shown in Fig. 5b. The southeastward component appeared to be stationary in the southwestern Pacific, whereas the eastward component extended to the eastern Pacific roughly following the equator (Fig. 5c–d).

In summary, the equatorial thermocline depth variation of an El Niño Modoki (CP-El Niño) demonstrated an east–

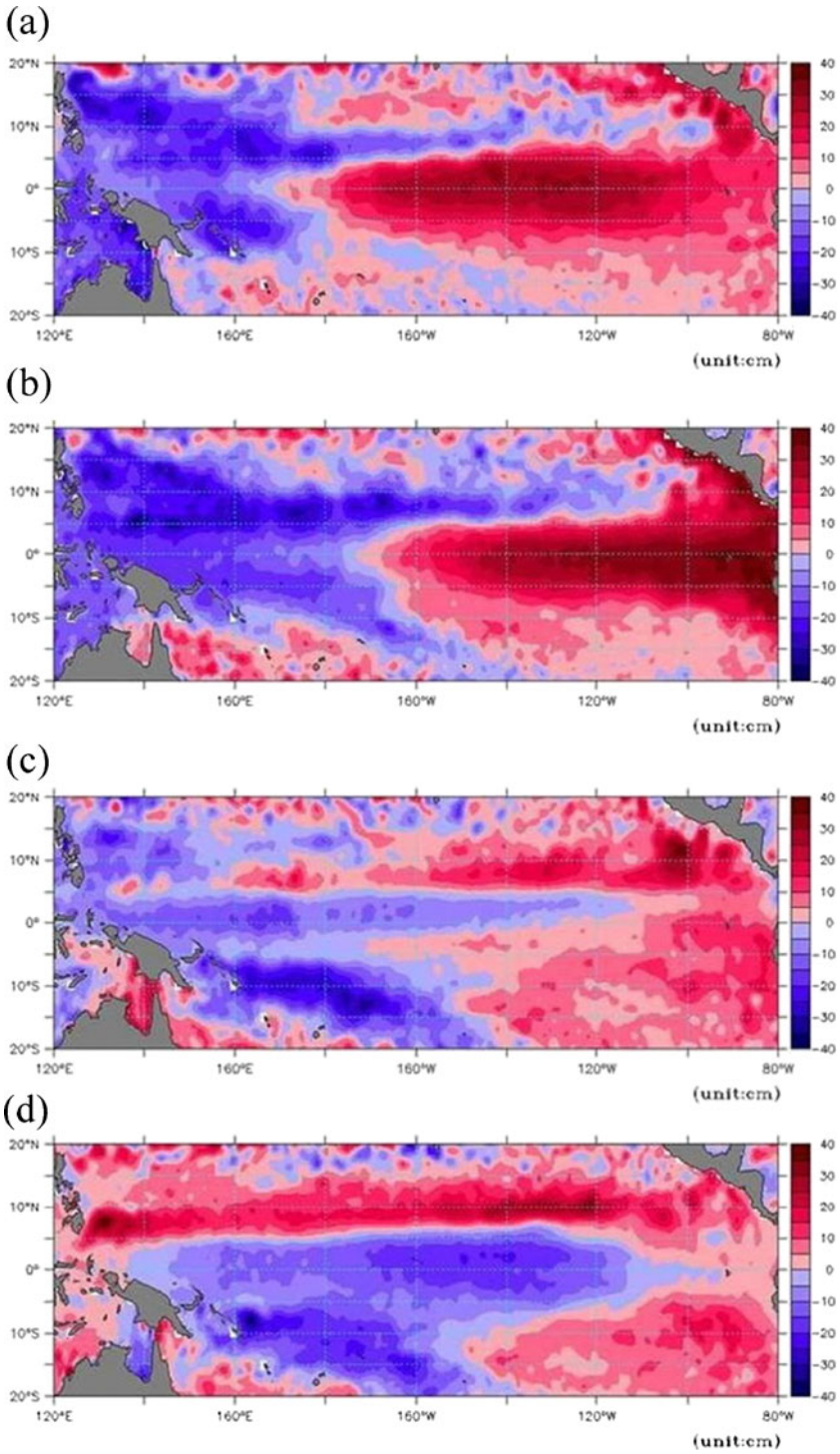

Fig. 5 Same as Fig. 3 except in **a** September 1997, **b** December 1997, **c** March 1998, and **d** June 1998

west seesaw oscillation. However, in addition to the east–west oscillation, the EP-El Niño displayed unusual behavior in the way the D20 tilted, with an additional north–south seesaw oscillation between approximately 15° N and 15° S. From September to December when the EP-El Niño was developing, the D20 in the eastern Pacific was almost 100 m deeper than the corresponding D20 in the west-central Pacific. The D20 in the northwestern Pacific was about 50 m shallower than in the southwestern Pacific (Fig. 4b). After the peak of the EP-El Niño, the sharp east–west D20 gradient gradually diminished or even reversed. The meridional seesaw oscillation also reversed and the D20 in the northwestern Pacific became deeper than that in the southwestern Pacific (Fig. 4d). The meridional seesaw oscillation could be interpreted as the movements of the elevated D20. The elevated D20 in the northwestern Pacific migrated

toward the southeast. Part of it was trapped at the equator, becoming eastward-propagating Kelvin waves. For EP-El Niño events, the ENSO oscillator theory should take the north–south oscillation within 15° N–15° S into consideration.

3.3 Forcing mechanism

The meridional oscillation of the thermocline depth could be explained by the effect of the tropical wind stress curl pattern. Previous studies have shown that the Intertropical Convergence Zone (ITCZ) tends to move southward during El Niño events (e.g., Rasmusson and Carpenter 1982; Philander 1985; Wolter and Timlin 1993), and so does the zero wind stress curl line (the nodal line separates into positive curls to the north and negative curls to the south). However, the meridional migration of the zero wind stress curl line differs among El Niño events. Figure 6a shows the wind stress curl averaged over the southwestern Pacific (150° E–180° E, 5° S–7° S) during the mature phase of El Niño events between 1980 and 2010. We focused on the west-central Pacific because the tropical wind anomaly associated with the ENSO is large over the western to central Pacific Ocean (Deser and Wallace 1990; Jin 1997a), indicating that the main ocean–atmosphere coupling occurs in the west-central equatorial Pacific rather than in the eastern equatorial Pacific (as demonstrated by Clarke et al. 2007). A large and positive curl was observed during the mature phases of the 1982/1983 and 1997/1998 El Niño (EP type) events (Fig. 6a). Wind stress curl patterns composited by the mature phase of the two EP-El Niño events and the other El Niño Modoki (CP-El Niño) events are shown in Fig. 6b and c, respectively. During the mature phase of the EP-El Niño events, the zero wind stress curl line shifted southward and large positive curls occupied the western equatorial region. Different wind stress curl patterns will trigger distinct thermocline variations within the tropical Pacific, which will in turn affect the SST evolution between the two types of El Niño.

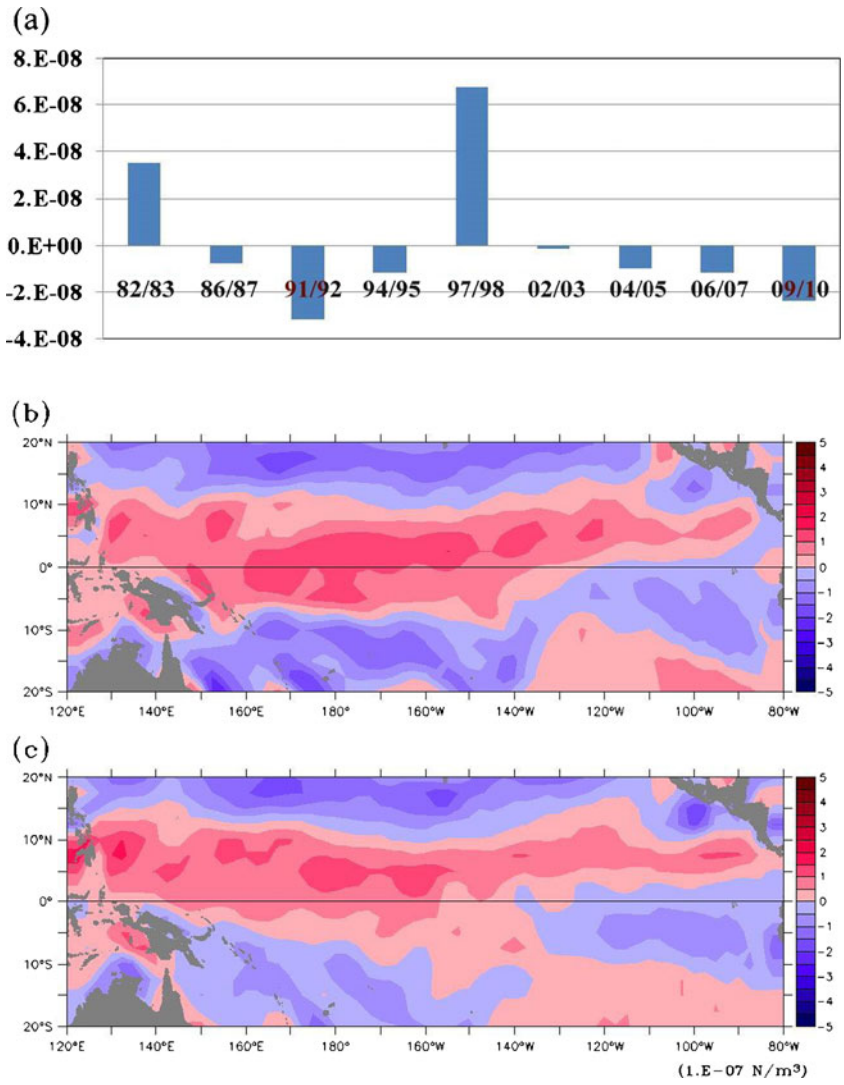

Fig. 6 **a** Wind stress curl averaged over the southwestern Pacific (150–180° E, 5–7° S) during the mature phase of an El Niño between 1980 and 2010. Wind stress curl pattern composited for the mature phase of **b** the EP-El Niño events and **c** the CP-El Niño events. Contour interval for wind stress curl is 0.5×10^{-7} Nm^{-3}

During the onset of El Niño Modoki (CP-El Niño) events, a positive wind stress curl occurred in the northwestern Pacific and a negative curl was located to the southwest, which agrees well with the preconditions of the warm water discharge process. However, during the onset of EP-El Niño events, large positive curls in the northwestern Pacific induced an upwelling through Ekman pumping and raised the thermocline depth (figures not shown). A raised D20 was clearly observed in the northwestern Pacific (Fig. 4a). During mature EP-El Niño events, the zero wind stress curl line migrated southward toward the equator. A strong positive wind stress curl occurred in the northwestern Pacific and a rather strong negative curl was located to the southwest, both elevating the thermocline depth and inducing the WWV discharge. As a result, the D20 in the western Pacific was raised (Fig. 4b). This phenomenon prevailed in the western Pacific, which agrees with several recent studies which concluded that the main region of ENSO air–sea interaction occurs in the west-central Pacific (e.g., Clarke et al. 2007). When evolving into the decay phase, the zero wind stress curl line began to shift northwards, while a negative wind stress curl occurred near the equatorial region. The negative curl in the northwestern Pacific deepened the thermocline and resulted in a recharge of the WWV, while the negative curl in the southwestern Pacific elevated the thermocline depth and then induced a discharge of the WWV. The elevated thermocline depth appeared to occur in the northwestern Pacific during the event onset, extending to the equator during the mature phase. During the decay phase, it separated into two portions extending to the southern Pacific Ocean and propagating eastward along the equator, respectively.

Furthermore, in addition to the meridional migration of the zero wind stress curl line, the intensity of wind stress curl was much stronger in an EP-El Niño event than an El Niño Modoki (CP-El Niño) event as shown in Fig. 6b and c. The stronger wind stress curl resulted in stronger thermocline depth variations in an EP-El Niño. The negative D20 anomalies of an EP-El Niño extended to 70 m and were much larger than the D20 anomalies of a CP-El Niño (20 m), resulting in SST anomalies for the EP type being stronger than those in the CP type. Both the large magnitude and the meridional seesaw pattern of the oscillation were characteristics of EP-El Niño, and the meridional seesaw oscillation of the equatorial thermocline was not only a necessary condition, but also a sufficient precondition of an EP-El Niño.

3.4 The distinct decay phase of the EP El Niño

The 1982/1983 EP-El Niño displayed a similar evolution pattern to the 1997/1998 EP-El Niño except during the decay phase. In March 1983, after the peak of the El Niño, a negative D20 anomaly in the southern Pacific reached 50 m, which was much deeper than its counterpart trapped at the equator (~10 m; Fig. 7a). The pattern deviated from that in March 1998, when the D20 anomalies were almost equal (~40 m) between the southern Pacific and equator (see Fig. 4c). Such differences affect the evolution of the cold event following the El Niño. For example, the 1982/1983 warm event was brought to a normal state, whereas the 1997/1998 El Niño was followed by 3 years of La Niña. In 1982/1983, because the negative D20 anomaly in the equator was relatively weak, it almost disappeared during its eastward propagation as Kelvin waves (Fig. 7b). Consequently, the negative SST anomaly in 1983 could not be defined as a La Niña using the Nino 3.4 index (5° S–5° N, 120° W–170° W). However, in 1997/1998 the negative D20 anomaly at the equator was large and became stronger as it propagated eastward during the decay phase, while the anomaly in the southern Pacific became weaker (Fig. 4d). From August to September 1998, negative D20 anomalies at the equator occupied the region of 120° W–150° W and thereafter spread westward. This induced a particularly strong negative SST anomaly, followed by 3 years of cold events.

Although thermocline variations could lead to distinct decay patterns, the direct effects are likely to be wind stress curl patterns in the equatorial Pacific. Wind stress curl shifted northward far away from the equator during both EP-El Niños, but their pattern in the southern equatorial Pacific was different. During the decay phase in 1982/1983, a negative curl occurred south of the equatorial region (red rectangle in Fig. 8a). However, in the 1997/1998 decay phase, positive wind stress curls together with strong easterly trade winds occurred in the southern equatorial Pacific Ocean (Fig. 8b). The wind stress curl variation was connected to the ITCZ migration. During the decay phase of an El Niño, the ITCZ generally starts to retreat northward. This movement of the ITCZ was faster during 1997/1998 than in 1982/1983 (figure

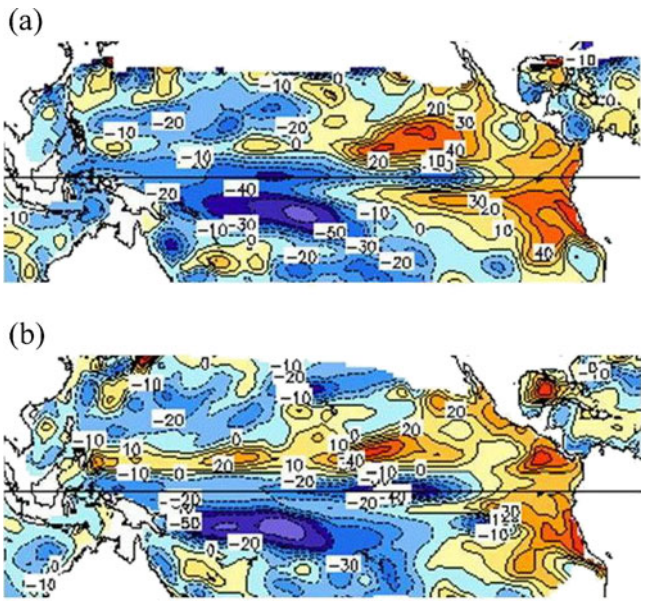

Fig. 7 The modeled 20 °C isotherm depth anomalies in **a** March 1983 and **b** June 1983. Contour interval is 10 m

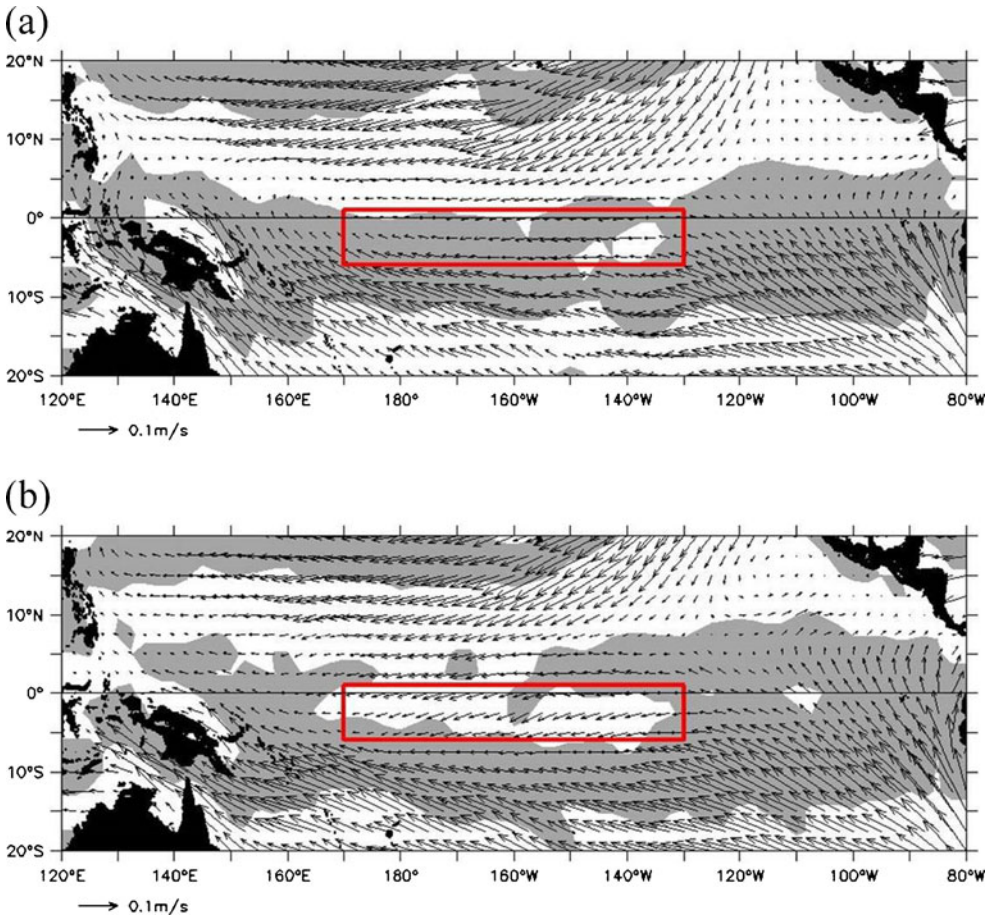

Fig. 8 Wind stress curl (*shading*) and wind stress (*vector*) averaged from May to July in **a** 1983 and **b** 1998. Negative contours are *shaded*. Vector scale is 0.1 m/s. The *red rectangle* encloses the region from 1° N–6° S, 170° E–130° W in the central equatorial Pacific

not shown). Recent research has demonstrated how the retreat of an equatorial ITCZ abruptly terminates El Niño events, bringing back easterly winds accompanied by a cooling at the equator (Lengaigne and Vecchi 2009). Thus, in 1997/1998, easterly trade winds appeared immediately after the mature phase, due in part to the faster retreat of the ITCZ. The trade winds cooled the SST in the equatorial Pacific and immediately initiated the transition phase into a La Niña event. However, in 1982/1983, the ITCZ retreated relatively slowly and the trade winds did not appear quickly enough to cool down the SST. As a result, the transition phase returned to normal conditions. Specifically, the weak negative thermocline anomalies under the prolonged warming conditions were not powerful enough to instantly convert the 1982/1983 El Niño into a La Niña.

4 Concluding remarks

Two distinct patterns of El Niño evolution were identified using the tropical 20 °C isotherm depth of the GODAS product. Both patterns of evolution were confirmed by satellite altimeter sea surface height anomaly data. The thermocline depth variation of El Niño Modoki (CP-El Niño) events displayed an east–west seesaw oscillation in the equatorial Pacific. In addition to the east–west oscillation, the EP-El Niño also displayed an extra north–south seesaw oscillation between approximately 15° N and 15° S. This unique feature only appeared during an EP-El Niño and was not recorded in earlier El Niño studies. We demonstrated that the wind stress curl over the western and central Pacific was closely linked to the north–south seesaw oscillation of the equatorial thermocline depth during an EP-El Niño. This argument does not contradict the standard recharge–discharge paradigm (Jin 1997a, b). Because the definition of an ENSO event is based on the zonal (east–west) redistribution of warm water along the equator, the recharge and discharge of warm water are not necessarily associated with the local wind stress curl variability. The wind stress curl fluctuation triggers distinct thermocline depth variations within the tropical Pacific Ocean, modulating the evolution of the SST evolution in the two types of El Niño. Thus, EP-El Niño events, with both east–west and north–south seesaw oscillations are not only produced by basin-wide thermocline variations, but are also influenced by the wind stress curl in the equatorial Pacific. Hence, the EP-El Niño also involves strong air–sea interactions. The meridional seesaw oscillation of thermocline variation is a major factor in inducing the distinct evolution patterns of the two types of El Niño.

Thermocline depth anomalies in the equatorial Pacific were stronger in 1997/1998 than 1982/1983, which resulted in distinct differences during the decay phases between the two EP-El Niño events, and subsequently affected the SST variations and the evolution of the following La Niña event. The state of the thermocline in the equatorial Pacific Ocean can be attributed to the rate of the ITCZ migration. The 1997/1998 El Niño with a rapidly retreating ITCZ abruptly terminated the warm event and immediately became a La Niña event, whereas the slow retreat of the ITCZ in 1982/1983 terminated the warm event at a much slower rate resulting in a return to a normal phase.

Acknowledgments The authors would like to thank the Editor, Dr. Yukio Masumoto, and the anonymous reviewers for their careful review of the manuscript and detailed suggestions to improve the manuscript. The authors are also grateful to D. J. Shea and colleagues from the NCAR for assistance in processing the GODAS outputs. Authors CRW and LCW were supported by the National Science Council, Taiwan, under grants NSC 100-2119-M-001-029-MY5 and NSC 101-2917-I-003-002.

References

Ashok K, Behera S, Rao AS, Weng H, Yamagata T (2007) El Niño Modoki and its teleconnection. J Geophys Res 112, C11007. doi:10.1029/2006JC003798

Behringer DW, Xue Y (2004) Evaluation of the global ocean data assimilation system at NCEP: The Pacific Ocean. Eighth Symposium on Integrated Observing and Assimilation Systems for Atmosphere, Oceans, and Land Surface, AMS 84th Annual Meeting, Washington State Convention and Trade Center, Seattle, Washington, 11–15

Braganza K (2008) Seasonal climate summary southern hemisphere (autumn 2007). La Niña emerges as a distinct possibility in 2007. Aust Met Mag 57:65–75

Cane MA, Zebiak SE, Dolan SC (1986) Experimental forecasts of El Niño. Nature 321:827–832

Clarke AJ, Gorder SV, Colantuono G (2007) Wind stress curl and ENSO discharge/recharge in the equatorial Pacific. J Phys Oceanogr 37:1077–1091

Deser C, Wallace JM (1990) Large-scale atmospheric circulation features of warm and cold episodes in the tropical Pacific. J Clim 3:1254–1281

Conkright ME, Levitus S, O'Brien T, Boyer TP, Stephens C, Johnson D, Baranova O, Antonov J, Gelfeld R, Rochester J, Forgy C (1999) World ocean database 1998 CD-ROM data set documentation, Version 2.0. NODC Internal Report 14, 116pp

Ji M, Leetmaa A (1997) Impact of data assimilation on ocean initialization and El Niño prediction. Mon Wea Rev 125:742–753

Jin FF (1997a) An equatorial ocean recharge paradigm for ENSO. Part I: conceptual model. J Atmos Sci 54:811–829

Jin FF (1997b) An equatorial ocean recharge paradigm for ENSO. Part II: a tripped-down coupled model. J Atmos Sci 54:830–847

Kanamitsu M, Ebisuzaki W, Woolen J, Yang SK, Hnilo JJ, Fiorino M, Potter GL (2002) NCEP-DOE AMIP-II reanalysis (R-2). Bull Amer Meteor Soc 83:1631–1643

Kao HY, Yu JY (2009) Contrasting eastern–Pacific and central–Pacific types of El Niño. J Clim 22:615–632. doi:10.1175/2008JCLI2309.1

Kessler WS (1990) Observations of long Rossby waves in the northern tropical Pacific. J Geophys Res 95(C4):5183–5217

Kistler R, Kalnay E, Collins W, Saha S, White G, Woollen J et al (2001) The NCEP–NCAR 50-Year Reanalysis: Monthly means CD-ROM and documentation. Bull Amer Meteor Soc 82:247–267

Kug JS, Jin FF, An SI (2009) Two types of El Niño events: cold tongue El Niño and warm pool El Niño. J Clim 22:1499–1515. doi:10.1175/2008JCLI2624.1

Kug JS, Choi J, An SI, Jin FF, Wittenberg AT (2010) Warm pool and cold tongue El Niño events as simulated by the GFDL 2.1 coupled GCM. J Clim 23:1226–1239

Larkin NK, Harrison DE (2005) Global seasonal temperature and precipitation anomalies during El Niño autumn and winter. Geophys Res Lett 32, L16705. doi:10.1029/2005GL022860

Lengaigne M, Vecchi GA (2009) Contrasting the termination of moderate and extreme El Niño events in coupled general circulation models. Climate Dyn. doi:10.1007/s00382-009-0562-3

Lukas R (2001) Pacific equatorial currents. In: Steele JH, Thorpe SA, Turekian KA (eds) Encyclopedia of ocean sciences. Academic, London

Luo JJ, Yamagata T (2001) Long-term El Niño–Southern Oscillation (ENSO)-like variation with special emphasis on the South Pacific. J Geophys Res 106:22211–22227

McPhaden MJ, Delcroix T, Hanawa K, Kuroda Y, Meyers G, Picaut J, Swenson M (2001) The El Niño/Southern oscillation (ENSO) observing system. Observing the ocean in the 21st century. In: Koblinsky CJ and Smith NR (Eds) Australian Bureau of Meteorology, p 231–246

Meinen CS, McPhaden MJ (2000) Observations of warm water volume changes in the equatorial Pacific and their relationship to El Niño and La Niña. J Clim 13:3551–3559

Philander SGH (1985) El Niño and La Niña. J Atmos Sci 42:652–662

Rasmusson EM, Carpenter TH (1982) Variations in tropical sea surface temperature and surface wind fields associated with the Southern Oscillation/El Niño. Mon Wea Rev 110:354–384

Wang B, Wu R, Lukas R (1999) Roles of the western North Pacific wind variation in thermocline adjustment and ENSO phase transition. J Meteor Soc Japan 77:1–16

Wang LC, Wu CR (2012) Modulation of the equatorial currents by the two types of El Niño events. Atmosphere–Ocean. doi:10.1080/07055900.2012.744294

Wolter K, Timlin MS (1993) Monitoring ENSO in COADS with a seasonal adjusted principal component index. Proc. 17th Climate Diagnostics Workshop. Norman, OK, NOAA/NMC/CAC, 52–57

Wyrtki K (1974) Sea level and the seasonal fluctuations of the equatorial currents in the western Pacific Ocean. J Phys Oceanogr 4:91–103

Yu JY, Kao HY (2007) Decadal changes of ENSO persistence barrier in SST and ocean heat content indices: 1958–2001. J Geophys Res 112, D13106. doi:10.1029/2006JD007654

Yu JY, Kim ST (2010) Three evolution patterns of Central–Pacific El Niño. Geophys Res Lett 37, L08706. doi:10.1029/2010GL042810